Supporting Information

Interfacial Charge Transfer Driven by Surface Termination-Controlled Ti_2C MXene for Enhanced Hydrogen Storage in Magnesium

Min Gyu Kim[a], ShinYoung Kang[b], Brandon C. Wood[b], and Eun Seon Cho[a]*

[a] Department of Chemical and Biomolecular Engineering, Korea Advanced Institute of Science and Technology (KAIST), Daejeon 34141, Republic of Korea.

[b] Laboratory for Energy Application for the Future (LEAF), Lawrence Livermore National Laboratory, Livermore, California 94550, United States.

*corresponding author: escho@kaist.ac.kr

Experimental Section

Chemicals and Materials

Ti powder (99.5%, 325 mesh), Al powder (99.5%, 325 mesh), Li foil (99.9%, 0.75mm thick×19mm wide), TiC (99.5%), LiCl (99.995%, ultra-dry), NaCl (99.99%, ultra-dry), LiF (99.98%, metal basis) and $CdCl_2$ (99.998%, ultra-dry) were purchased from Alfa Aesar. Pyrene (98 %), biphenyl (99.5 %, ReagentPlus), KCl (99.99 %, AnhydroBeads), HCl (37 %, ACS reagent), *N*-methyl formamide (NMF, 99 %) were purchased from Sigma-Aldrich. THF (99.5 %, HPLC) was purchased from DAEJUNG and purified using a solvent purification system before use. Bis(cyclopentadienyl) magnesium (Cp_2Mg, 99.99 %) was purchased from Strem Chemicals.

Synthesis of Ti_2AlC MAX phase

Ti_2AlC MAX phase was synthesized from TiC, Ti and Al was synthesized via a molten-salt approach as previously reported.[1] TiC (10.7 mmol, 0.641 g), Ti (10.7 mol, 0.512 g) and Al (12.9 mol, 0.347 g) (1:1:1.2 molar ratio) powders were thoroughly mixed with NaCl (43.2 mmol, 2.525 g) and KCl (43.2 mmol, 3.221 g) salts (4:4 molar ratio) using mortar and pestle in the Ar glovebox. The resultant mixture was placed in a boat alumina crucible. Subsequently, it was loaded in a tube furnace and heated at 1080 °C for 3 h under Ar flow. After the reaction was completed, the product was washed with DI water to remove the residual salts, and the final product was dried under vacuum at 60 °C.

Synthesis of ML-Ti_2CCl_2 MXene

ML-Ti_2CCl_2 MXene was synthesized using the modified molten-salt etching method.[2] Ti_2AlC MAX phase (3.71 mmol, 0.5 g) was thoroughly mixed with $CdCl_2$ (22.3 mmol, 4.082 g), KCl (7.42

mmol, 0.553 g), LiCl (9.34 mmol, 0.396 g) (1:6:2:2.515 molar ratio) using mortar and pestle in Ar glove box. The resultant mixture was placed in an alumina crucible and packed in a furnace tube in the glove box. Subsequently, it was moved onto a tube furnace and heated at 610 °C for 6 h under a flow of Ar. After the reaction was completed, the product was treated with concentrated aqueous HCl (12.1 M, 40 ml) to remove the residual salts and Cd metal followed by washing with deionized water until pH becomes neutral. The final product was collected after drying under vacuum at 60 °C.

Synthesis of DL-Ti_2CCl_2 MXene

ML-Ti_2CCl_2 was delaminated using organolithium reagent lithium-pyrene (LiPy). LiPy solution was prepared by dissolving pyrene (3.36 mmol, 0.6796 g) and Li foil (3.36 mmol, 0.02332 g) in THF (15 ml). Ti_2CCl_2 (0.2 g) was immersed in LiPy solution and stirred for 48 hours in Ar filled glovebox. The Li-intercalated Ti_2CCl_2 was washed with THF 3 times (10,000 rpm, 20 min), followed by vacuum drying overnight. The resulting intercalated powder was taken out from a glovebox and dispersed in NMF (20 ml), followed by ultrasonication for 1 hour (<10 °C to minimize oxidation). Subsequently, the supernatant was collected by centrifuging at 240 g for 20 min to remove multilayer MXene and impurities. The supernatant was decanted to the other conical tube, and a stable MXene colloidal solution was obtained. Subsequently, 4 times volume of THF was added to reduce dispersibility of delaminated MXene nanosheets. Finally, the resultant mixture was centrifuged (10,000 rpm, 20 min) to precipitate the delaminated Ti_2CCl_2 (DL-Ti_2CCl_2) and washed with fresh THF 3 times (10,000 rpm, 20 min), followed by vacuum drying at 40°C overnight for further use.

Synthesis of Ti_2CT_x MXene

Ti_2CT_x MXene was synthesized by a LiF/HCl method.[3] The etching solution was prepared by adding LiF (27.8 mmol, 0.722 g) to 10 ml of 9 M HCl and stirring at 300 rpm for 5 min. Ti_2AlC powder (3.71 mmol, 0.5 g) was gradually added and stirred for 48 h at room temperature. The acidic solution was washed with a copious amount of deionized water by centrifuge until it reaches pH 6–7. During the repeated washing cycle, dark-purple supernatants were observed, indicating the initiation of delamination. After pH of solution reaches near neutral, the acidic mixture in a conical tube was vigorously shaken by hand for 10 min. The solution was centrifuged (3,500 rpm, 1 h), followed by the collection of dark supernatants. Finally, the collected supernatant was centrifuged (10,000 rpm, 20 min) to precipitate the delaminated Ti_2CT_x, followed by vacuum drying at 60°C overnight.

Synthesis of Mg@DL-Ti_2CCl_x

The synthesis of Mg composites was performed in an Ar-filled glovebox. Biphenyl (11.2 mmol, 1.733 g) and Li (15.6 mmol, 0.108 g) was added into THF (48 ml), and the solution was stirred for 2 h. DL-Ti_2CCl_2 was added into THF (in a concentration of 1 mg ml^{-1}) and sonicated for 1 h. Cp_2Mg (6 mmol, 0.924 g) was dissolved in THF (9 ml) and stirred for 30 min. The resulting solution was mixed with MXene dispersion (48 ml) and stirred for 30 min. The mixed solution was poured into a lithium biphenyl (LiBp) solution and reacted for 2 h with stirring. The final product (Mg@DL-Ti_2CCl_x) was washed by centrifugation (10,000 rpm, 20 min) with THF several times to remove residual reagents and impurities until supernatant is clear, followed by vacuum drying overnight and collected. Mg@Ti_2CT_x was synthesized via same method using Ti_2CT_x instead of DL-Ti_2CCl_2.

LiBp-treatment of a series of MXenes

Each MXene–ML-Ti_2CCl_2 (0.1 g), DL-Ti_2CCl_2 (0.1 g), Ti_2CT_x (0.1 g)–was treated with LiBp solution in the same condition. LiBp solution was prepared by dissolving biphenyl (3.36 mmol, 0.518 g) and Li foil (3.36 mmol, 0.02332 g) in THF (15 ml). Each compound was immersed in a separate LiBp solution and stirred for 24 h. The resulting compound was washed by centrifugation (10,000 rpm, 20 min) with THF several times until supernatant is clear, followed by vacuum drying overnight and collected.

Material Characterization

The X-ray diffraction (XRD) patterns were obtained using Rigaku SmartLab High Resolution Powder X-ray diffractometer with Cu Kα X-ray source (λ=1.5406 Å). The transmission electron microscopy (TEM), selected-area electron diffraction (SAED), high-angle annular dark field (HAADF) and energy-dispersive X-ray spectrometry (EDS) images were collected on FEI Tecnai G2 F30 S-Twin operated at 300 kV and FEI Talos F200X. The scanning electron microscope (SEM) imaging were performed with Hitachi SU-8230. The Raman spectra were collected with a Horiba Jobin Yvon LabRAM ARAMIS and Si wafer was used for calibration. The samples were excited using a 514 nm light source with laser power set to 1% for measurements and using 50x long path objective and 1000 mm^{-1} grating. The X-ray photoelectron spectroscopy (XPS) was performed on a Thermo VG Scientific K-alpha using monochromatic Al Kα source (1486.8 eV) and vacuum transfer holder was used to prevent severe oxidation of samples. Peak fitting of XPS spectra was performed with Thermo Scientific Avantage software. A Tougaard background and asymmetric Lorentzian line shape was used for better fitting of transition metal-based conductive samples.[4, 5] Adventitious carbon peak of C 1s was set at 284.8 eV to compensate charge-induced shifts. XRD, TEM, SEM, Raman spectroscopy, XPS analysis were carried out at KAIST Analysis

Center for Research Advancement (KARA). Ti L-edge near edge X-ray absorption fine structure (NEXAFS) measurements were performed at Pohang Light Source (PLS) 10D XAS KIST beamline.

Hydrogen Absorption and Desorption Measurements

Hydrogen sorption measurements were acquired with a Sievert-type Setaram PCTPro system. The sample cell temperature was controlled by PID controller and heating jacket. Powdered samples were loaded into a stainless holder under the protection of Ar and connected to the instrument. Hydrogen absorption and desorption kinetics were obtained at different temperatures under 15 bar and 0 bar of hydrogen, respectively.

Calculation of Kinetic Energy Barrier

The activation energies were derived using the Arrhenius law from the isothermal kinetic curves obtained at three different temperatures. The rate of reaction was calculated with slope of the curve which was smoothed using the Lowess method.[6, 7] Finally, activation energies were calculated from a linear fit of 1/T against the ln (rate) for each stage of (de)hydrogenation. The kinetic energy barrier was also calculated by fitting the Johnson-Mehl-Avrami (JMA) equation for comparison.[8, 9] The fraction of (de)hydrogenated Mg or MgH_2 was determined from saturated value from kinetic curve.

Theoretical Calculation

We constructed interface models between MgH_2 nanoparticle with a radius of ~1 nm and DL-Ti_2CCl_x sheet (x = 0.0, 0.5, 1.0, and 1.5). The simulation box consists of 36 formula units of Ti_2CCl_x and 15 formula units of MgH_2, and its hexagonal cell has a dimension of a = b = 19.4 Å

and c > 25 Å to ensure enough vacuum thickness in the c-axis direction. The density functional theory (DFT) calculations were performed using the Vienna Ab Initio Simulation Package (VASP). [10] The generalized gradient approximation (GGA)-based DF2 functional accounting for the van der Waals dispersion interactions was used within the projected augmented wave (PAW) approach. [11-13] The kinetic energy cutoff for the plane-wave basis set was set to 520 eV. Lattice parameter fixed to the bulk values and atomic positions are fully optimized until energy converges to 10^{-4} eV and force converges to < 0.05 eV/Å. Model structures and charge densities are visualized using VESTA and OVITO.[14, 15]

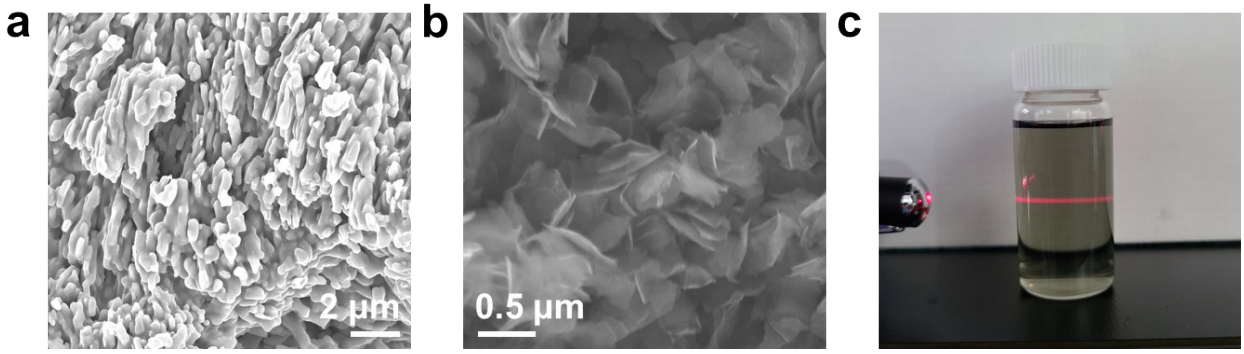

Figure S1. SEM image of (a) Ti_2AlC MAX phase and (b) DL-Ti_2CCl_2. (c) Tyndall effect of stable DL-Ti_2CCl_2 dispersion in NMF.

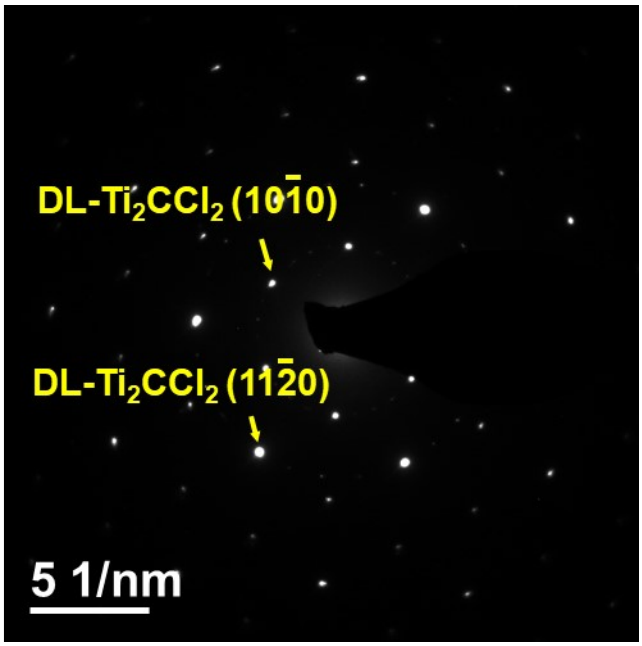

Figure S2. SAED pattern of DL-Ti_2CCl_2 sheet.

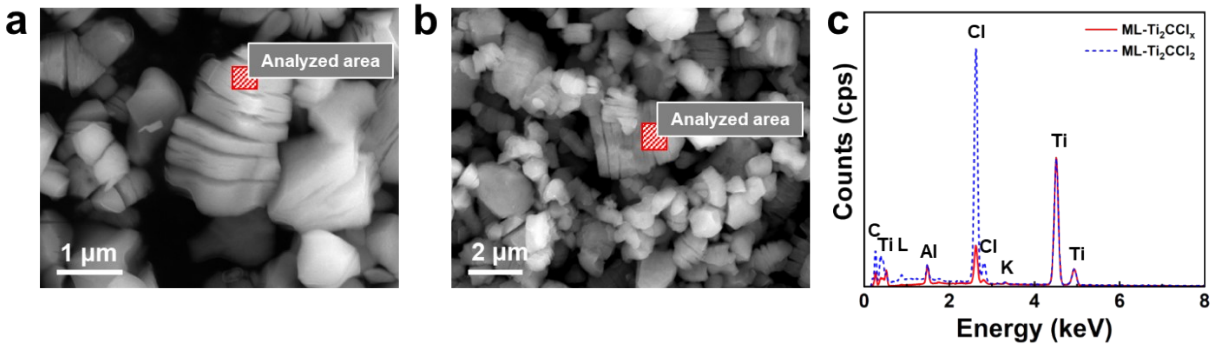

Figure S3. SEM image of (a) ML-Ti_2CCl_2 and (b) ML-Ti_2CCl_x, and (c) the corresponding energy-dispersive spectroscopy (EDS) analysis showing the reduced amount of Cl.

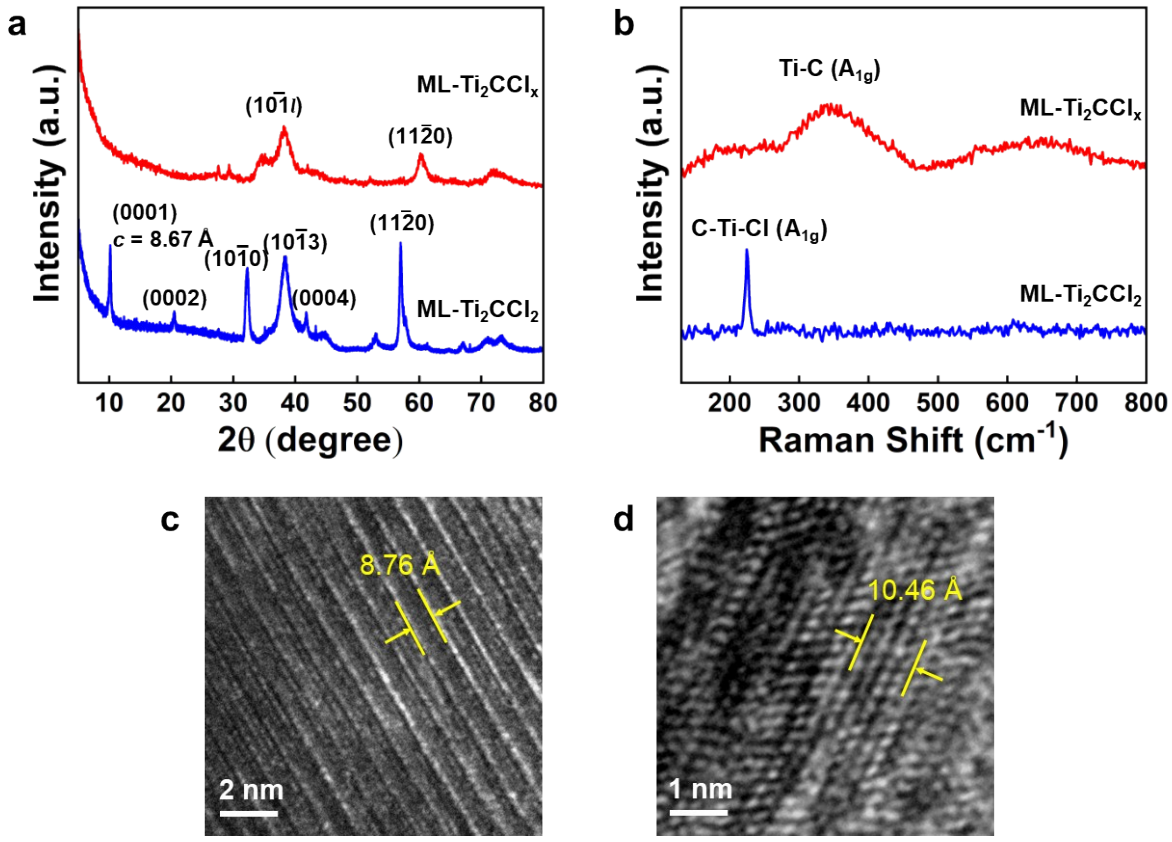

Figure S4. (a) XRD patterns and (b) Raman spectra of ML-Ti_2CCl_2 and ML-Ti_2CCl_x. HRTEM image of (c) ML-Ti_2CCl_2 and (d) ML-Ti_2CCl_x.

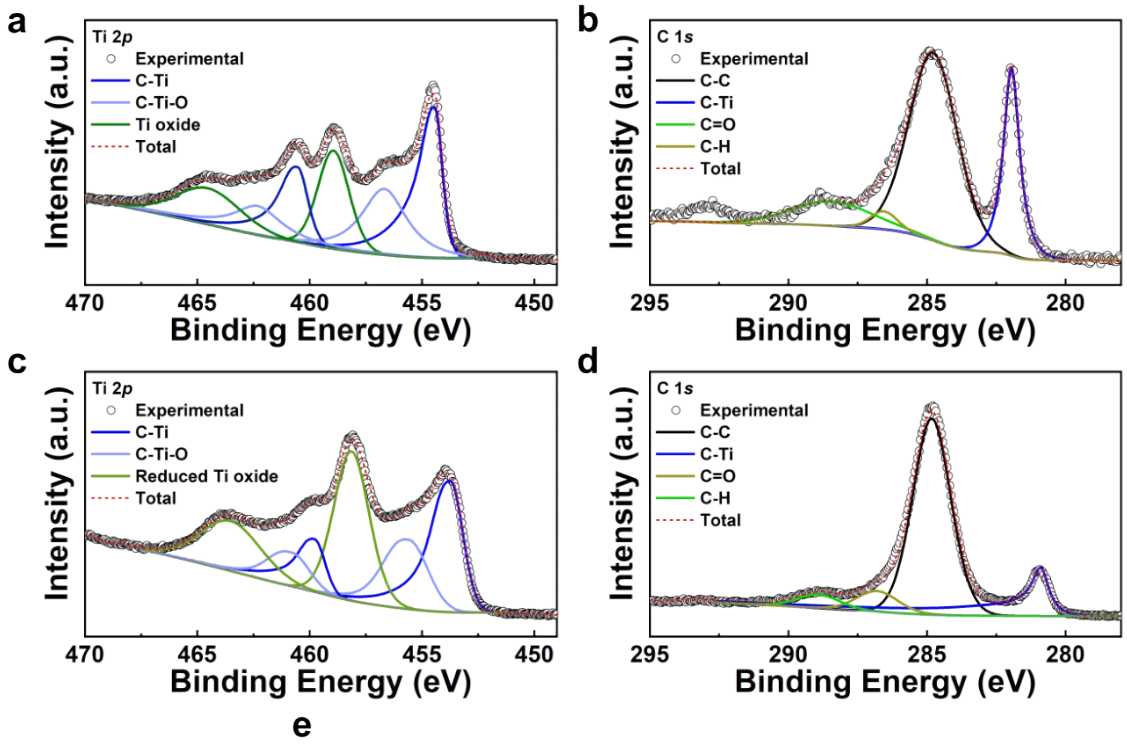

Figure S5. Ti 2*p* and C 1*s* XPS spectra of (a, b) DL-Ti_2CCl_2 and (c, d) DL-Ti_2CCl_x. The peak shift observed in (a) and (c) related to Ti oxide is speculated to occur due to the reduction of amorphous surface oxide on the surface of the MXene.

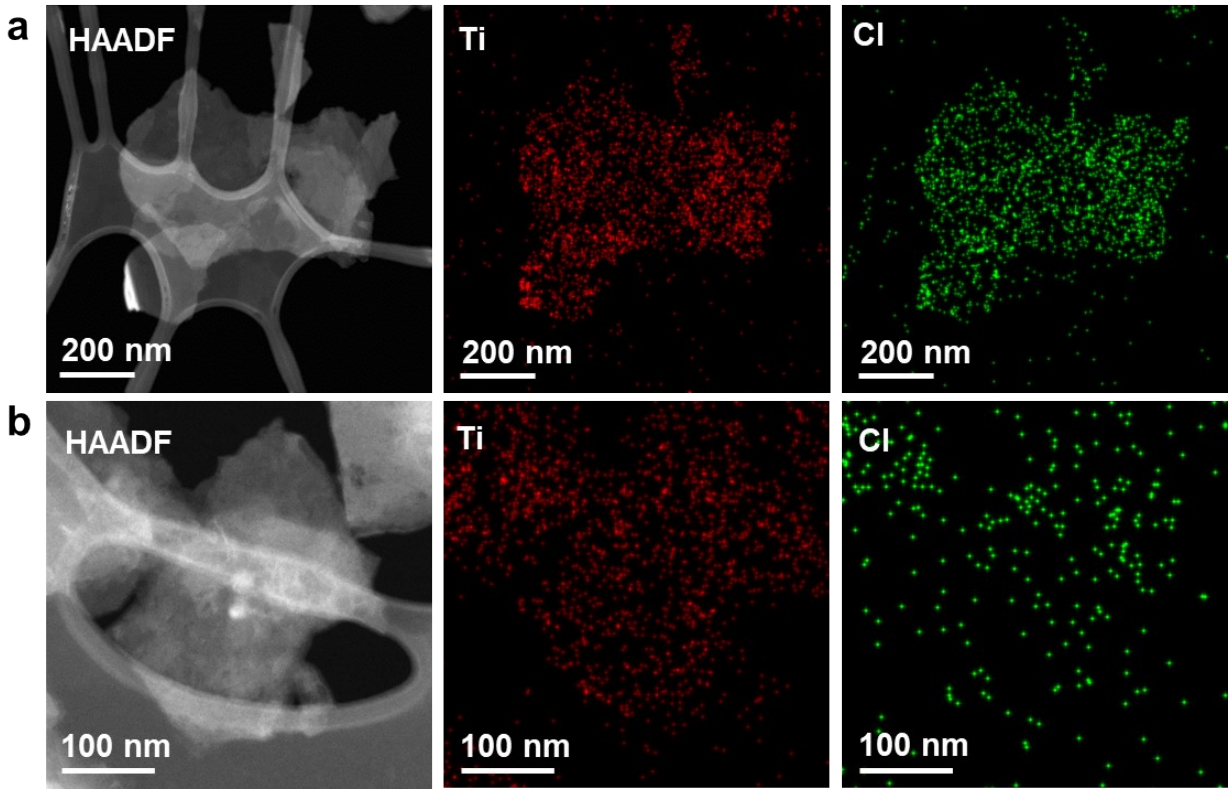

Figure S6. HAADF image and the corresponding EDS mapping of (a) DL-Ti_2CCl_2 and (b) DL-Ti_2CCl_x

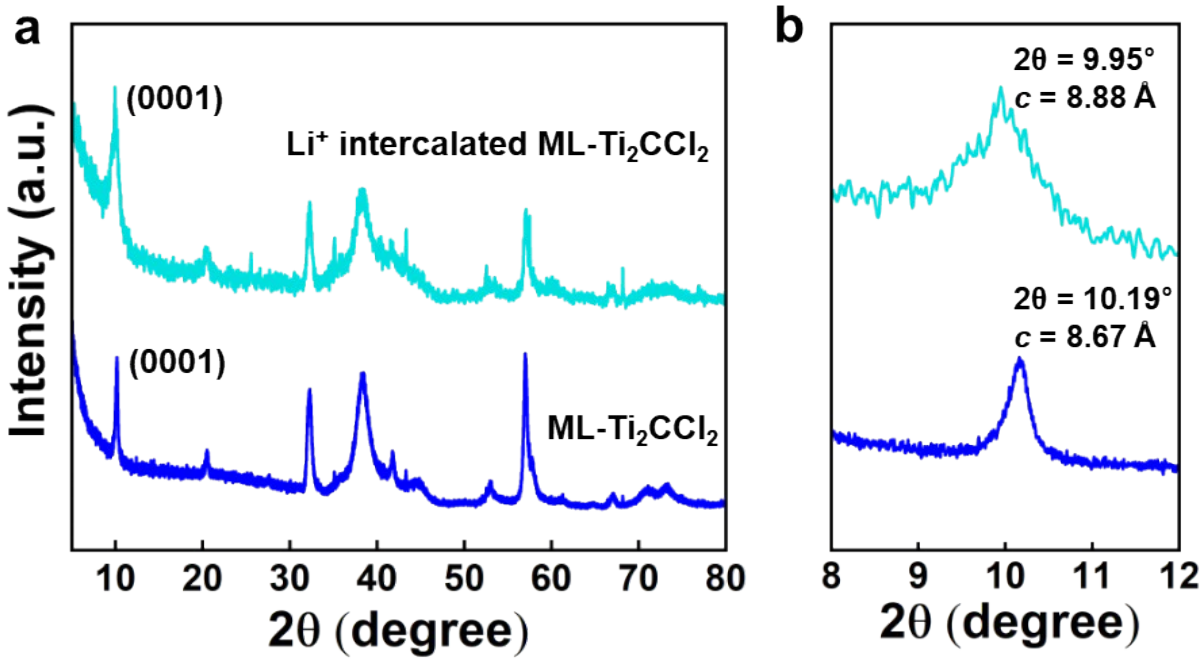

Figure S7. (a) XRD patterns and (b) their magnification of in the range of 2θ = 8–12° for ML-Ti_2CCl_2 and Li^+-intercalated ML-Ti_2CCl_2 after LiPy treatment.; a Li^+-intercalated ML-Ti_2CCl_2 which represents an intermediate state prior to the delamination into DL-Ti_2CCl_2 is measured to demonstrate the Li^+-intercalation.

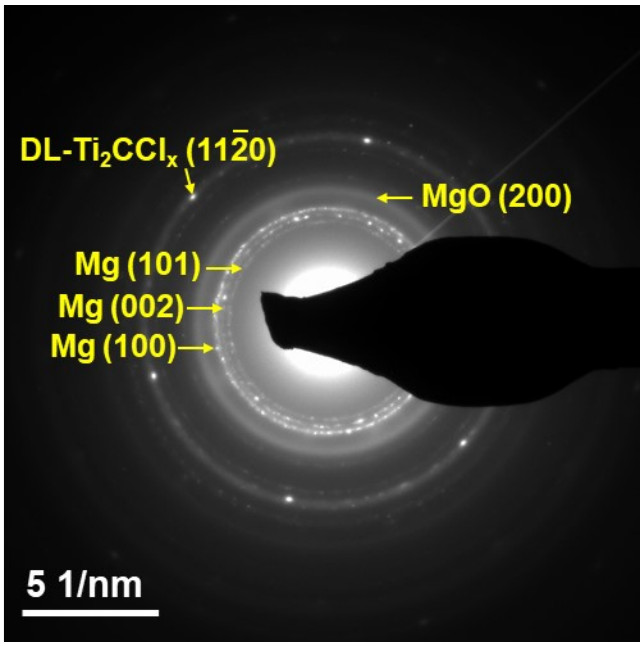

Figure S8. SAED pattern of Mg@DL-Ti_2CCl_x. The diffuse ring pattern corresponds to MgO formation, presumably resulting from surface oxidation during the sample transfer process.

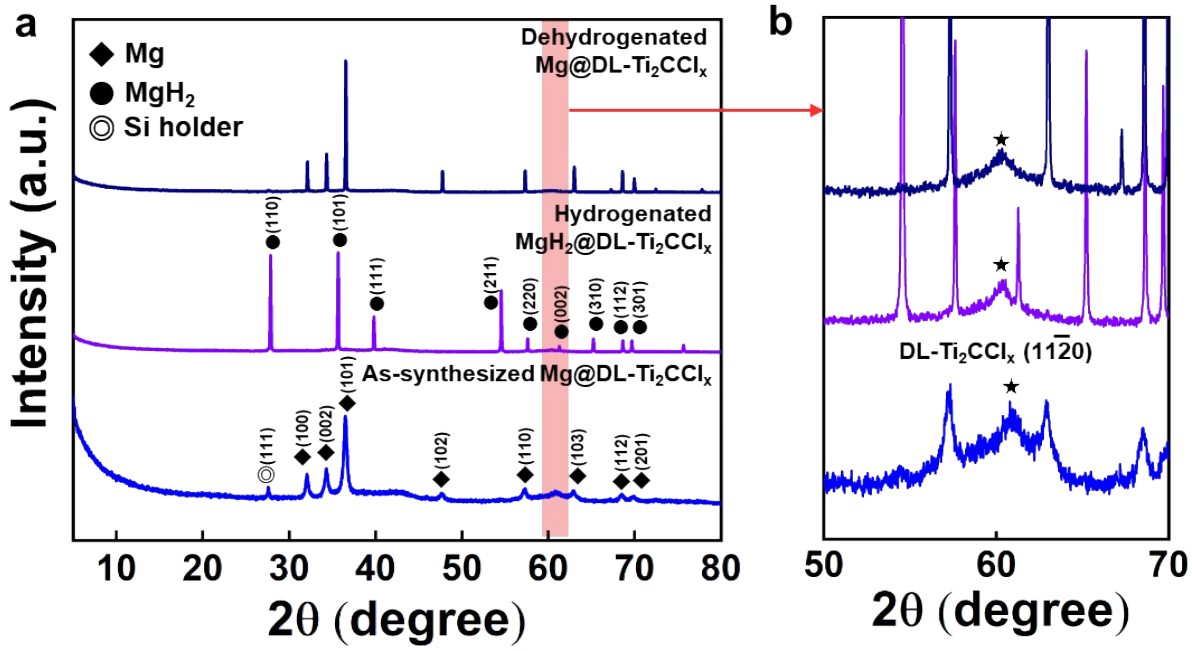

Figure S9. (a) XRD patterns and (b) their magnification in the range of 2θ = 50–70° for as-synthesized Mg@DL-Ti_2CCl_x and (de)hydrogenated Mg@DL-Ti_2CCl_x after H_2 sorption cycles.

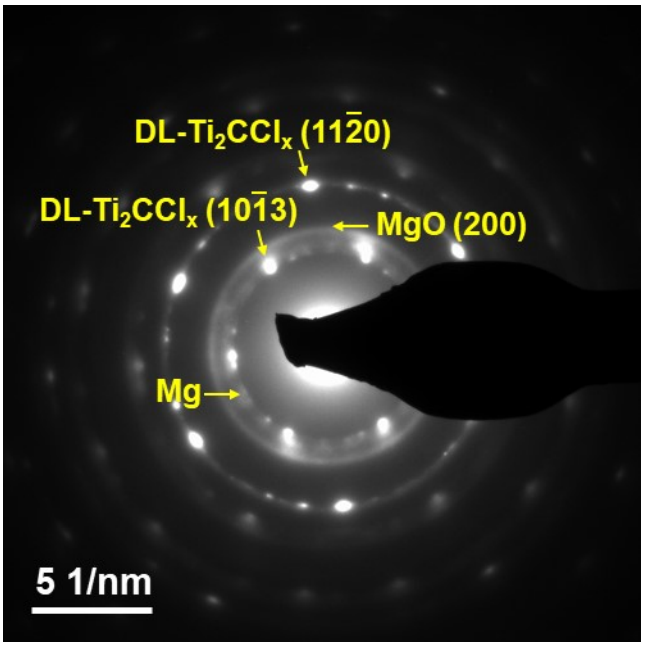

Figure S10. SAED pattern of Mg@DL-Ti_2CCl_x after hydrogen sorption cycle.

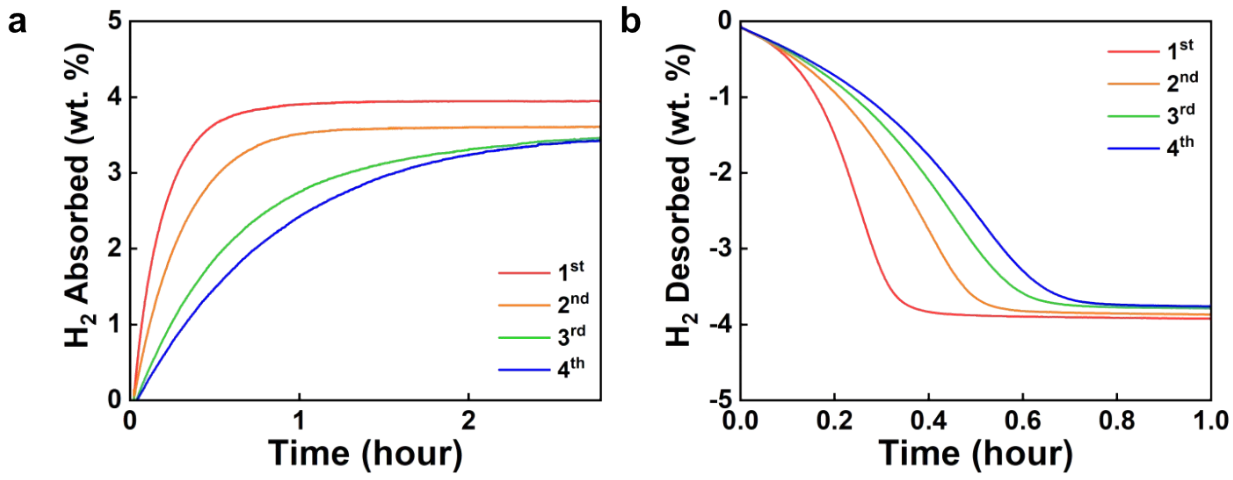

Figure S11. Hydrogen sorption kinetics of $Mg@Ti_2CT_x$: (a)absorption at 200 °C under 15 bar of H_2 and (b) desorption at 300 °C under 0 bar of H_2.

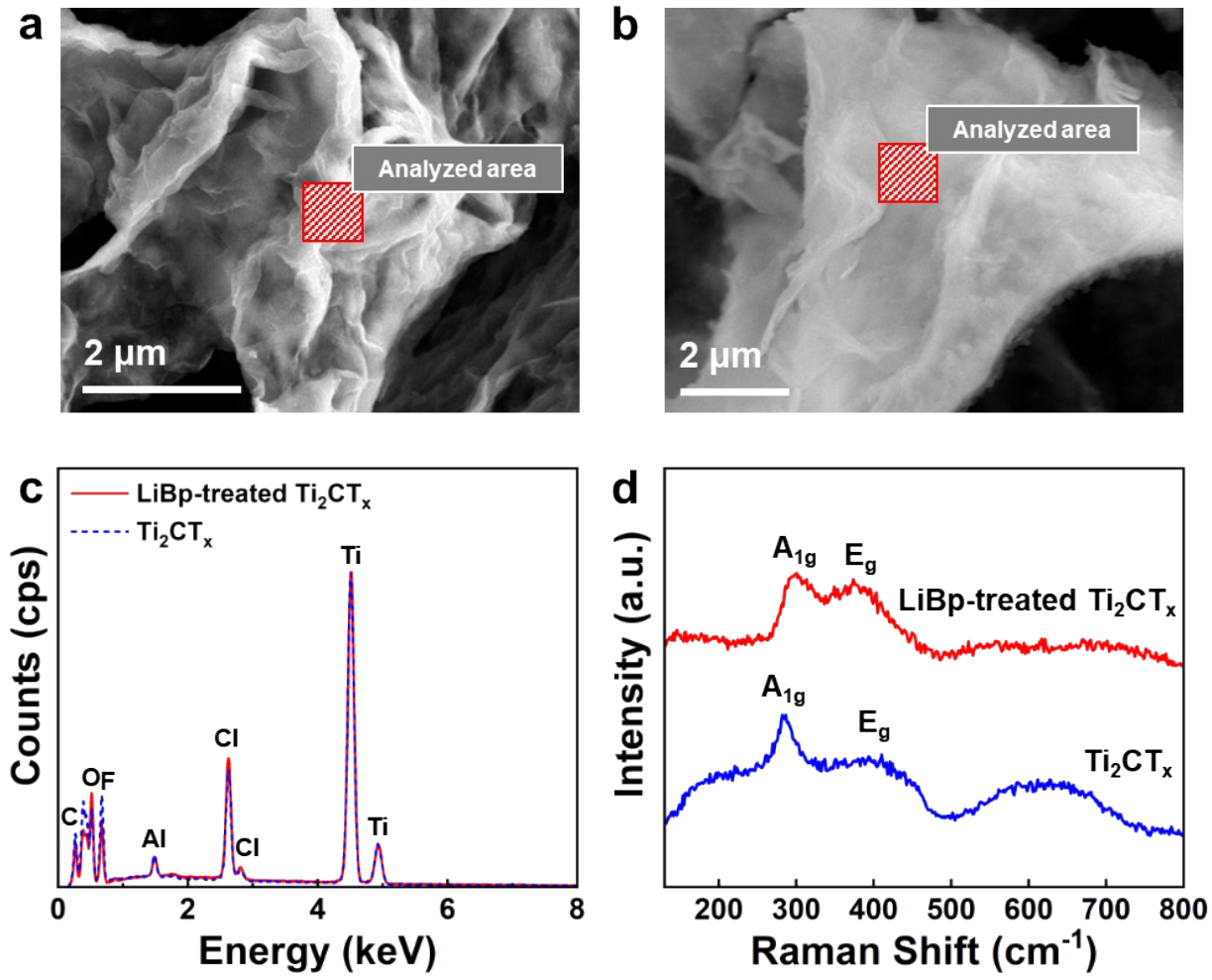

Figure S12. SEM image of (a) Ti_2CT_x and (b) LiBp-treated Ti_2CT_x with (c) the corresponding energy-dispersive spectroscopy (EDS) analysis showing minimal changes in elemental composition and (d) Raman spectra

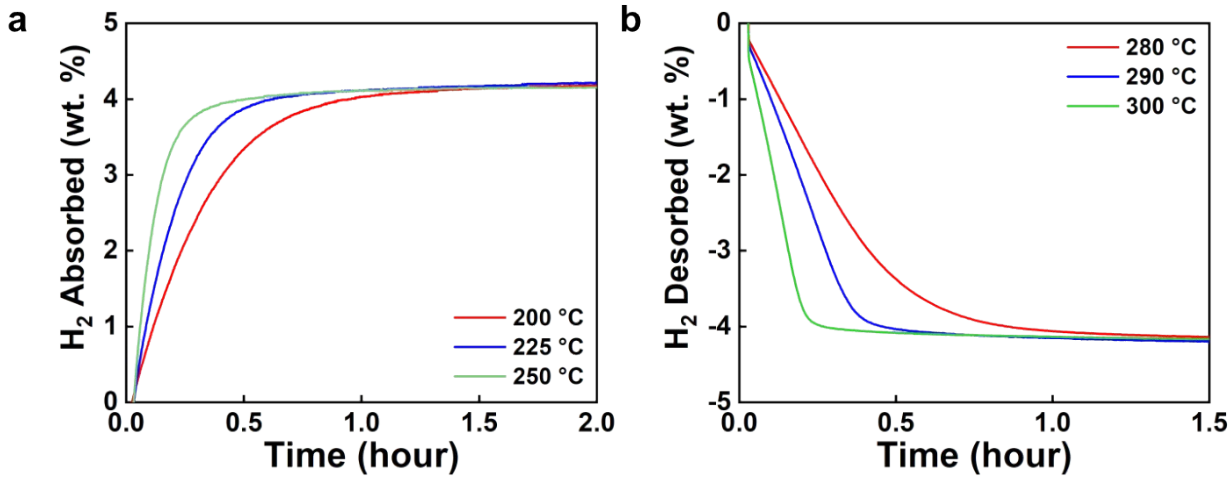

Figure S13. Isothermal hydrogen sorption kinetics of Mg@DL-Ti_2CCl_x at three different temperatures: (a) absorption 200 °C, 225 °C and 250 °C under 15 bar of H_2 and (b) desorption at 280 °C, 290 °C and 300 °C under 0 bar of H_2.

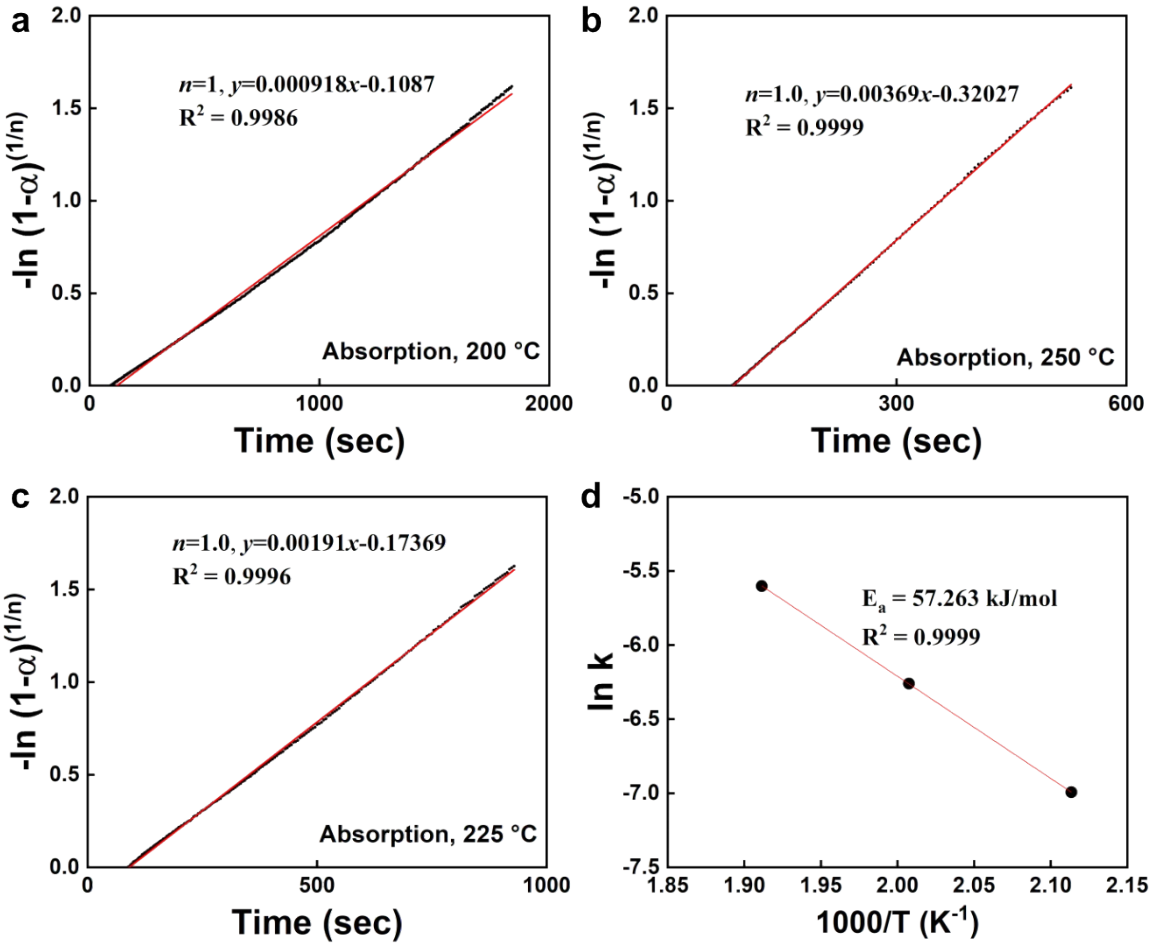

Figure S14. (a–c) JMA fitting of isothermal H_2 absorption of Mg@DL-Ti_2CCl_x at 200 °C, 225 °C and 250 °C. (d) Determination of absorption activation energy by plotting logarithmic rate constant versus 1000/T.

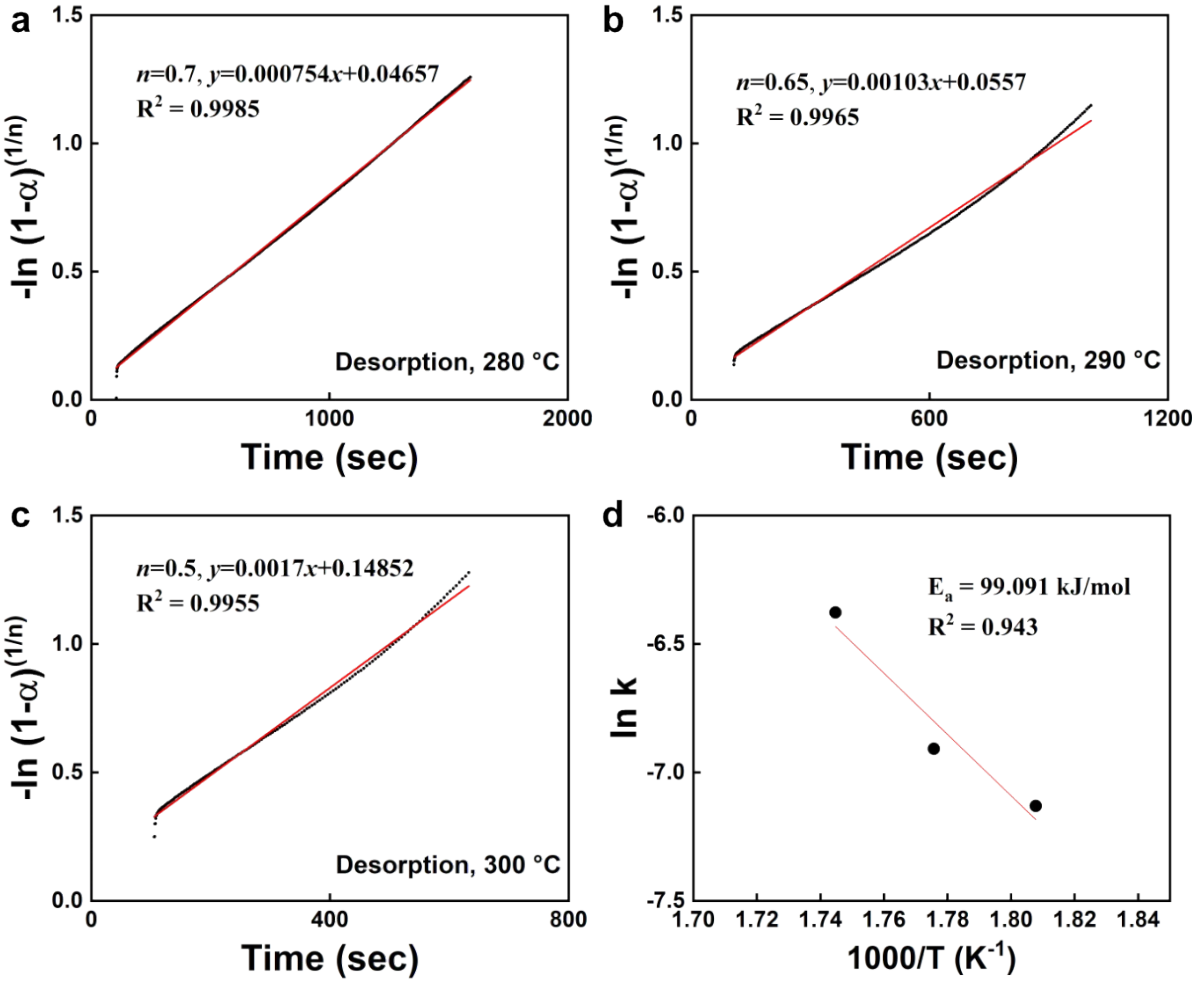

Figure S15. (a–c) JMA fitting of isothermal H_2 desorption of Mg@DL-Ti_2CCl_x at 280 °C, 290 °C and 300 °C. (d) Determination of desorption activation energy by plotting logarithmic rate constant versus 1000/T.

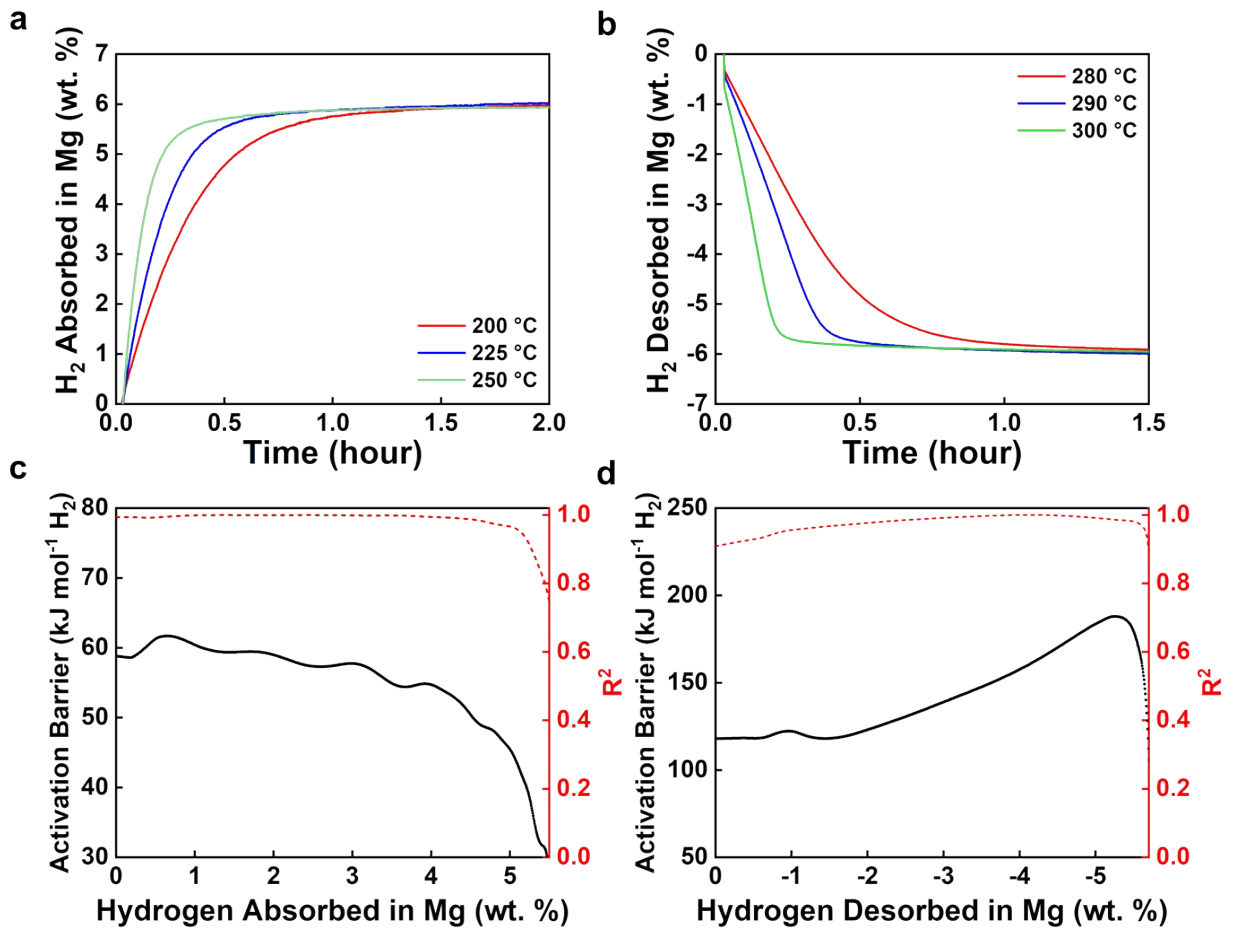

Figure S16. Isothermal hydrogen sorption kinetics of Mg@DL-Ti_2CCl_x at three different temperatures based on active material (Mg) mass: (a) absorption 200 °C, 225 °C and 250 °C under 15 bar of H_2 and (b) desorption at 280 °C, 290 °C and 300 °C under 0 bar of H_2. Activation barrier for (c) absorption and (d) desorption as a function of absorbed and desorbed wt. % H_2, in Mg respectively.

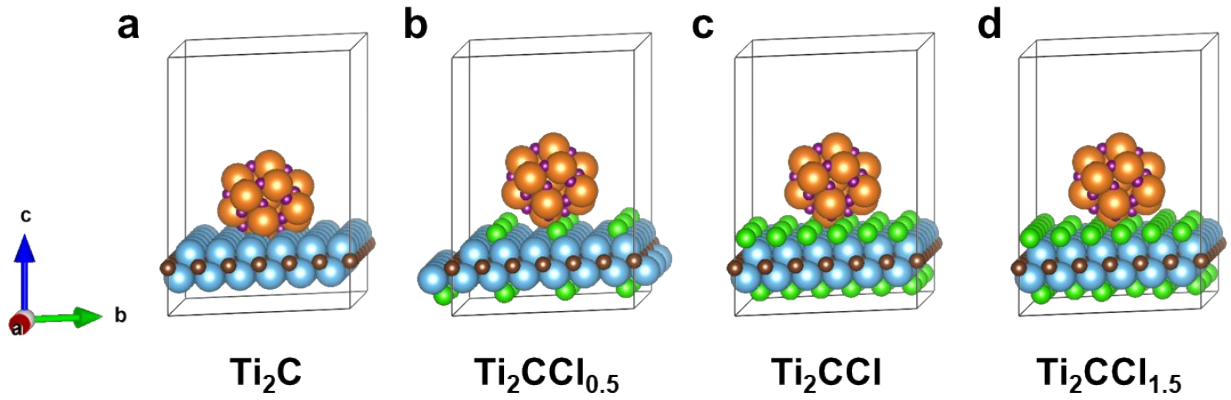

Figure S17. MgH_2@DL-Ti_2CCl_x interface models used for DFT calculations. (a) x = 0, (b) x = 0.5, (c) x = 1, and (d) x = 1.5. Large orange and small purple spheres in the spherical particle are Mg and H atoms in MgH_2 nanoparticles, respectively. Large blue, small brown and small green spheres are Ti, C, and Cl atoms in Ti_2CCl_x MXene sheets, respectively.

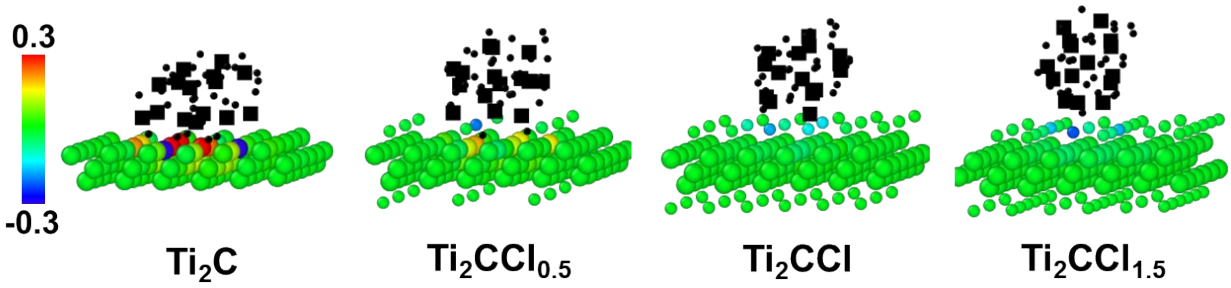

Figure S18. Bader charge states of Ti_2CCl_x in MgH_2@Ti_2CCl_x interface model with respect to isolated Ti_2CCl_x sheets. The reddish circles in the Ti_2CCl_x part especially at low Cl concentrations demonstrates the oxidation of some interface Ti atoms. Mg and H atoms are colored in black for simplicity.

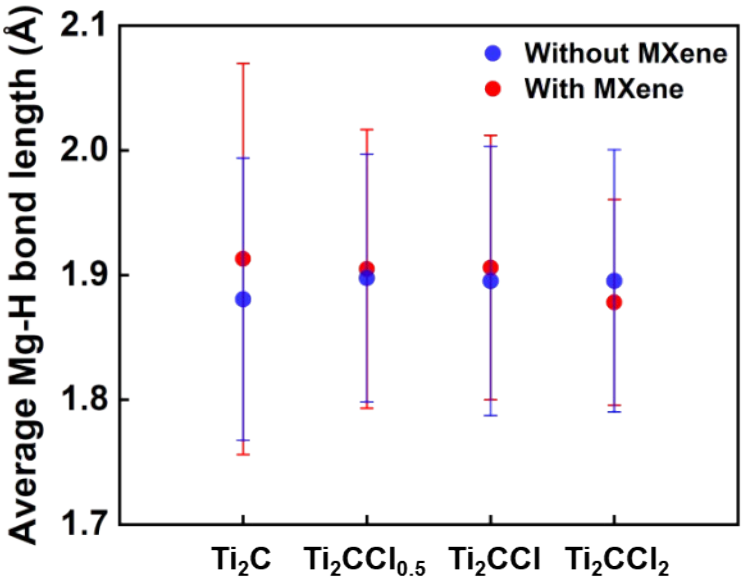

Figure S19. Elongation of Mg-H bond evaluated based on the DFT calculation depends on presence of MXene.

Element (at. %)	ML-Ti_2CCl_2	ML-Ti_2CCl_x
Ti	48.5	80.4
Cl	47.4	13.1
Al	3.4	5.2
K	0.7	1.3

Table S1. Elemental composition of ML-Ti_2CCl_2 and ML-Ti_2CCl_x from EDS spectra.

Element (at. %)	Ti_2CT_x	LiBp-treated Ti_2CT_x
Ti	31.7	32.1
O	35.1	42.3
F	25.7	18.3
Cl	6.3	6.9
Al	1.1	0.4

Table S2. Elemental composition of Ti_2CT_x and LiBp-treated Ti_2CT_x from EDS spectra.

REFERENCES

1 M. Li, J. Lu, K. Luo, Y. Li, K. Chang, K. Chen, J. Zhou, J. Rosen, L. Hultman and P. Eklund, *J. Am. Chem. Soc.*, 2019, **141**, 4730-4737.

2 V. Kamysbayev, A. S. Filatov, H. Hu, X. Rui, F. Lagunas, D. Wang, R. F. Klie and D. V. Talapin, *Science*, 2020, **369**, 979-983.

3 M. Alhabeb, K. Maleski, B. Anasori, P. Lelyukh, L. Clark, S. Sin and Y. Gogotsi, *Chem. Mater.*, 2017, **29**, 7633-7644.

4 V. Natu, M. Benchakar, C. Canaff, A. Habrioux, S. Celerier and M. W. Barsoum, *Matter*, 2021, **4**, 1224-1251.

5 D. Wang, C. Zhou, A. S. Filatov, W. Cho, F. Lagunas, M. Wang, S. Vaikuntanathan, C. Liu, R. F. Klie and D. V. Talapin, *Science*, 2023, **379**, 1242-1247.

6 Y. Cho, S. Kang, B. C. Wood and E. S. Cho, *ACS Appl. Mater. Interfaces*, 2022, **14**, 20823-20834.

7 E. S. Cho, A. M. Ruminski, Y. S. Liu, P. T. Shea, S. Kang, E. W. Zaia, J. Y. Park, Y. D. Chuang, J. M. Yuk and X. Zhou, *Adv. Funct. Mater.*, 2017, **27**, 1704316.

8 K.-J. Jeon, H. R. Moon, A. M. Ruminski, B. Jiang, C. Kisielowski, R. Bardhan and J. J. Urban, *Nat. Mater.*, 2011, **10**, 286-290.

9 E. S. Cho, A. M. Ruminski, S. Aloni, Y.-S. Liu, J. Guo and J. J. Urban, *Nat. Commun.*, 2016, **7**, 10804.

10 G. Kresse and J. Furthmüller, *Physical review B*, 1996, **54**, 11169.

11 J. P. Perdew, K. Burke and M. Ernzerhof, *Physical review letters*, 1996, **77**, 3865.

12 P. E. Blöchl, *Physical review B*, 1994, **50**, 17953.

13 K. Lee, É. D. Murray, L. Kong, B. I. Lundqvist and D. C. Langreth, *Physical Review B*, 2010, **82**, 081101.

14 K. Momma and F. Izumi, *Journal of applied crystallography*, 2011, **44**, 1272-1276.

15 A. Stukowski, *Modelling and simulation in materials science and engineering*, 2009, **18**, 015012.